Study on the electrochemical properties of cubic ordered mesoporous carbon for supercapacitors

Jun-Wei Lang, Xing-Bin Yan*, Xiao-Yan Yuan, Jie Yang, Qun-Ji Xue

State Key Laboratory of Solid Lubrication, Lanzhou Institute of Chemical Physics, Chinese Academy of Sciences, Lanzhou 730000, PR China

ABSTRACT

Highly ordered, three-dimensional (3D) cubic mesoporous carbon CMK-8 is prepared by a facile nanocasting approach using cubic mesoporous silica KIT-6 as starting template. Afterwards, in order to increase the active sites of surface electrochemical reactions and promote the wettability in aqueous electrolyte, a chemical surface modification is carried out on the CMK-8 by nitric acid treatment. Two electrodes are prepared from the CMK-8 and the acid-modified CMK-8 (H-CMK-8) and used as the active materials for supercapacitors. The unique 3D mesoporous network combined with high specific surface area makes the nano-channel surfaces of the CMK-8 carbon favorable for charging the electric double-layer, resulting in that the CMK-8 and the H-CMK-8 electrodes both show well supercapacitive properties. Furthermore, the specific capacitance of the CMK-8 can be further improved by acid treatment, so that the H-CMK-8 exhibits the largest specific capacitance of 246 F g^{-1} at a current density of 0.625 A g^{-1} in 2 M KOH electrolyte. Also, the two carbon electrodes both exhibit good cycling stability and lifetime. Therefore, based on the above investigations, such CMK-8 carbon, especially H-CMK-8 carbon can be a potential candidate for supercapacitors.

1. Introduction

It is now essential that high-performance, low-cost and environmentally friendly electrochemical energy storage systems are very important, in response to the needs of modern society and emerging ecological concerns [1,2]. Supercapacitors, as energy-storage/conversion device exhibiting energy density higher by orders of magnitude than conventional capacitors, and greater power density and longer cycling life than common batteries, have attracted considerable attention [3–5]. Perhaps most importantly, supercapacitors can be charged and discharged at high rates; they can be either by themselves as the primary power source or in combination with fuel cells or batteries to deliver the high power needed during acceleration and to recover the energy during braking [6,7].

Based on the principle of energy storage, the supercapacitors are classified as faradaic pseudocapacitors and electrical double-layer capacitors (EDLCs) [8]. As we know, transition metal oxides and conducting polymers which commonly corresponding to faradaic pseudocapacitors, and carbon materials which commonly corresponding to EDLCs have been used as supercapacitor electrode materials [9–11]. Although the energy densities of faradaic

pseudocapacitors are greater than those on EDLCs, the phase changes in the pseudocapacitance materials limit their lifetime and power density due to the faradic reaction [12]. Carbon, in its various forms, has been used as the most ideal materials for supercapacitors, aiming at high specific capacitance together with high power density [13–15]. Thus, there has been a great deal of research effort on boosting the energy performance of the carbon materials. The studies showed that the increase in capacitance of carbon materials is achieved mainly by the optimization of pore size, specific surface area and surface treatments to promote the wettability in an appropriate electrolyte solution [16,17].

The pore structure of carbon materials (micro-, meso- and macropore) may critically affect their physicochemical properties, specially serving as an electrode material involving the electrolyte accessibility, ion transportation, electron conductivity, etc. [18,19]. It is well-known that, the presence of ultramicropores that are inaccessible to the electrolyte ions, as well as the broad distribution of pore size, significantly decreases the specific capacitance of the carbon materials [20,21]. Compared with traditional carbon electrode materials, ordered mesoporous carbons (OMCs) possess well-ordered pore structure, narrow pore size distributions, high specific pore volume and high specific surface area, which can facilitate the ions diffusion. Therefore, OMCs seem to be attractive candidates as electrode materials for supercapacitors [22,23].

Up to now, various methods such as soft template replicating, hard template nanocasting and self-assembly have been successfully employed to prepare OMCs with different porous structures

[24]. Among them, a kind of ordered two-dimensional (2D) hexagonally mesoporous carbon, called as CMK-3, has been become the most widely investigated electrode material for EDLCs. CMK-3 is commonly prepared via a direct-templating nanocasting using a hexagonally ordered mesoporous silica SBA-15 as hard template, and CMK-3 is the faithful replica of the mesoporous structure of SBA-15 [25,26]. Otherwise, another kind of ordered 3D cubic mesoporous carbon, called as CMK-8, can be prepared through a faithful inverse replica from a mesoporous silica KIT-6, which exhibits a typical 3D cubic structure (*Ia3d* symmetry) consisting of an interpenetrating bicontinuous network of channels [27,28]. It is known that, ion transport is unidirectional in the 2D hexagonal systems, whereas cubic mesoporous systems are known to have better ion transport properties due to the higher degree of pore interconnectivity. So conceivably, the unique 3D network of CMK-8 could facilitate ion diffusion throughout the nanochannels without pore blockage, which probably makes the surface of CMK-8 favorable for charging the electric double-layer [29]. Nevertheless, little attention has been focused on the supercapacitor application of CMK-8 materials.

Herein, powdery CMK-8 carbon with highly ordered, 3D cubic mesostructured channels was prepared through hard-template nanocasting approach using KIT-6 silica as the mother template. Also, in order to increase oxygen-containing functional groups on the pore surface of the CMK-8 and promote its wettability in aqueous electrolyte, the CMK-8 was surface modified by treatment with nitric acid. The supercapacitive properties of the unmodified and acid-modified CMK-8 were first studied in this paper. The results showed that two materials both exhibited good supercapacitive properties, acid-modified CMK-8 especially. The maximum specific capacitance of $246\,F\,g^{-1}$ was obtained for the H-CMK-8 carbon electrode at a current density of $0.625\,A\,g^{-1}$ in 2 M KOH electrolyte. Furthermore, two materials both exhibited good cycling stability and lifetime after running 2000 cycles.

2. Experimental

2.1. Synthesis of cubic mesoporous silica KTI-6

The KIT-6 parent material was prepared by hydrothermal synthesis according to the established procedures [28]. In a typical experiment, 4.0 g of triblock copolymer Pluronic P123 (poly (ethylene oxide)-b-poly (propylene oxide)-b-poly (ethylene oxide), $EO_{20}PO_{70}EO_{20}$, $M_w = 5800\,g\,mol^{-1}$), was dissolved in a solution consisted of 144 ml of water and 7.9 g of 37 wt.% HCl with the aid of stirring at 35 °C for 4 h. 4.0 g of n-butanol was added in the above solution and the mixture was kept on stirring for 1 h. After that, 8.6 g of tetraethyl orthosilicate (TEOS) was added at once under vigorous stirring and the mixture was kept on stirring at 35 °C for 24 h. Subsequently, the mixture was transferred into a Teflon autoclave, covered, placed in an oven and aged at 100 °C for 24 h. After the hydrothermal treatment, the white solid product was filtered hot without washing and dried at 100 °C for 24 h in air. The as-synthesized solid was washed with a mixture of ethanol–HCl (90:10, V:V), filtered, washed with ethanol and dried at room temperature. Finally, the silica KIT-6 was obtained by the calcinations at 550 °C for 6 h in air with a heating rate of $1\,°C\,min^{-1}$.

2.2. Synthesis of cubic mesoporous carbon CMK-8

Mesoporous carbon CMK-8 was synthesized by the nanocasting process using sucrose as a precursor and mesoporous silica KIT-6 as hard template according to the literature [28]. Typically, 2.0 g KIT-6 was placed in a Schlenk flask, dehydrated at 150 °C in vacuum for 4 h, flushed with argon and cooled down to room temperature. At the same time, 2.5 g of sucrose was added to a mixture of 10 g of H_2O and 0.28 g of 97 wt.% H_2SO_4 with stirring. After the sucrose had dissolved completely, the KIT-6 was added and the mixture was kept on stirring for over night. The resultant viscous mixture was subsequently heated in an oven at 100 °C and 160 °C for 6 h, respectively. The resulting powder was mixed again with a sucrose solution consisting of 1.6 g sucrose, 0.18 g of 97 wt.% H_2SO_4 and 10 g of H_2O for the second-time impregnation. After being treated again at 100 °C and 160 °C for 6 h as before, carbonization was carried out in a tube furnace at 900 °C for 3 h at a heating rate of $1.0\,°C\,min^{-1}$ under vacuum. Finally, the CMK-8 was obtained by the removal of the silica template using 5 wt.% HF solution at room temperature.

2.3. Chemical modification of CMK-8

The CMK-8 carbon was chemical modification using HNO_3 solution. Briefly, 0.3 g of CMK-8 was suspended in 30 ml of concentrated HNO_3 (68 wt.%) and then refluxed at 60 °C for 2 h. After the mixture was cooled down to room temperature, it was filtered and washed with deionized water until the PH value of the filtrate was around 7. Then the product was dried at 80 °C for 24 h in air. The nitric-acid-modified CMK-8 carbon was denoted as H-CMK-8.

2.4. Structural characterization

Transmission electron microscopy (TEM) measurements were conducted on a JEM-2010 microscope operated at 200 kV, to reveal the ordered structure of the CMK-8 sample. The powdery CMK-8 was first dispersed in ethanol with the aid of sonication and then collected using a carbon-film-covered copper grid for TEM analysis. Small-angle powder X-ray diffraction (XRD) patterns were recorded by a Bruker D8 powder X-ray diffractometer using Cu Kα radiation. The chemical compositions of the samples were analyzed by Fourier transformation infrared spectroscopy (FTIR) using a Bruker IFS66V FTIR spectrometer. Nitrogen adsorption–desorption isotherm measurements were performed on a Micromeritics ASAP 2020 volumetric adsorption analyzer at 77 K. The Brunauer–Emmett–Teller (BET) method was utilized to calculate the specific surface area of each sample and the pore-size distribution was derived from the adsorption branch of the corresponding isotherm using the Barrett–Joyner–Halenda (BJH) method. The total pore volume was estimated from the amount adsorbed at a relative pressure of $P/P_0 = 0.99$. The surface functionality of the H-CMK-8 was analyzed on a Perkin-Elmer PHI-5702 multifunctional X-ray photoelectron spectroscope (XPS, physical Electronics, USA) using Al Kα radiation of 1486.6 eV as the excitation source.

2.5. Electrode preparation and electrochemical measurements

The working electrodes were prepared according to the method reported in the literature [30]. Typically, 80 wt.% of CMK-8/or H-CMK-8 was mixed with 7.5 wt.% of acetylene black (>99.9%) and 7.5 wt.% of conducting graphite in an agate mortar until a homogeneous black powder was obtained. To this mixture, 5 wt.% of poly (tetrafluoroethylene) was added with a few drops of ethanol. After briefly allowing the solvent to evaporate, the resulting paste was pressed at 10 MPa to nickel gauze with a nickel wire for an electric connection. The electrode assembly was dried for 16 h at 80 °C in air. Each carbon electrode contained about 8 mg of electroactive material and had a geometric surface area of about 1 cm^2.

The electrochemical measurements of each as-prepared electrode were carried out using an electrochemical working station (CHI660D, Shanghai, China) in a three-electrode system in 2 M KOH electrolyte at room temperature. A platinum gauze electrode and a saturated calomel electrode served as the counter
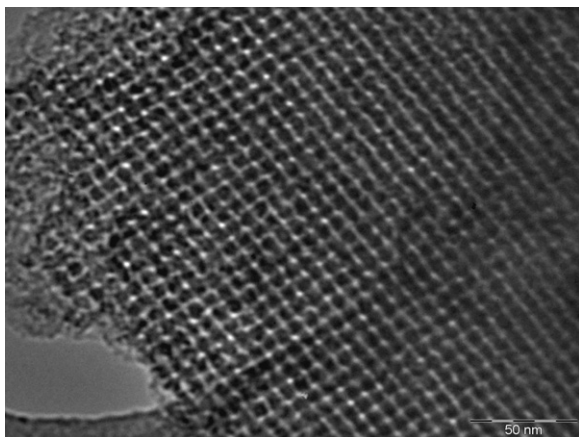
Fig. 1. TEM images of the CMK-8 taken along the [5 3 1] direction.
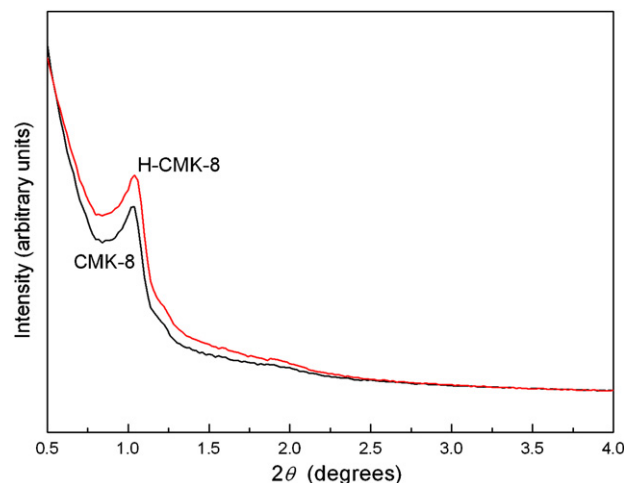

Fig. 2. The small-angle XRD patterns of the CMK-8 and the H-CMK-8.

electrode and the reference electrode, respectively. The cyclic voltammetry (CV) measurements were conducted with a potential window from −1.0 V to 0 V at different scan rates ranging from 10 mV s^{-1} to 50 mV s^{-1}. Electrochemical impedance spectroscopy (EIS) measurements were recorded from 10 kHz to 100 mHz with an alternate current amplitude of 5 mV. Galvanostatic charge/discharge measurements were run on from −1.0 V to 0 V at different current densities. Capacitance values were calculated form two methods: one is obtained from the cyclic voltammetry curves according to:

$$C = \frac{i}{v \times m} \quad (\text{F g}^{-1}) \tag{1}$$

where i is the average current (A), v is the scan rate (V s^{-1}) and m is the mass of active material in a electrode (g); another is calculated from the slopes of the discharge curves by the formula:

$$C = \frac{I}{(dE/dt) \times m} \approx \frac{I}{(\Delta E/\Delta t) \times m} \quad (\text{F g}^{-1}) \tag{2}$$

where C is the specific capacitance, I is the constant discharging current, dE/dt indicates the slope of the discharging curves, and m is the mass of the corresponding electrode material.

3. Results and discussion

3.1. Microstructure characterizations

Fig. 1 shows TEM image for the CMK-8 viewed along [5 3 1] direction. As the TEM image show, the CMK-8 exhibits a long-range-ordered mesostructure in the whole domain. As we know, the structure of the CMK-8 is exactly an inverse replica of KIT-6 which consists of 3D cubic (*Ia3d* symmetry) mesoporous tubes. The carbon nanorods are interconnected by spacer, which are constituted by the carbon that filled the channel-interconnecting micropores within the KIT-6 wall. Thus, the CMK-8 has an interpenetrating bicontinuous network of channels. Moreover, the H-CMK-8 has exactly the same TEM morphology as that of the CMK-8, which indicates that the acid-modification did not destroy the intrinsic ordered cubic *Ia3d* mesostructure of the CMK-8.

The ordered arrangement of the carbon nanorods in CMK-8 gives rise to the well-resolved XRD peak. Small-angle XRD patterns of CMK-8 and H-CMK-8 are shown in Fig. 2. Both the samples show a strong peak at 1.04°, which is indexed as (2 1 1) diffraction of the 3D cubic *Ia3d* symmetry [28]. Moreover, compared with the CMK-8, there is no obvious change in intensity and position of the peak for H-CMK-8. It further confirms that the ordered mesoporous

structure can be well preserved and the pore-size did not take place obvious change after the acid-modification.

The acid-modification of the CMK-8 carbon can affects significantly the surface functionality. The FTIR measurements were employed to monitor chemical composition changes on the channel surface of the CMK-8 before and after acid modification. Fig. 3a shows the FTIR spectra of CMK-8 and the H-CMK-8. A broad band
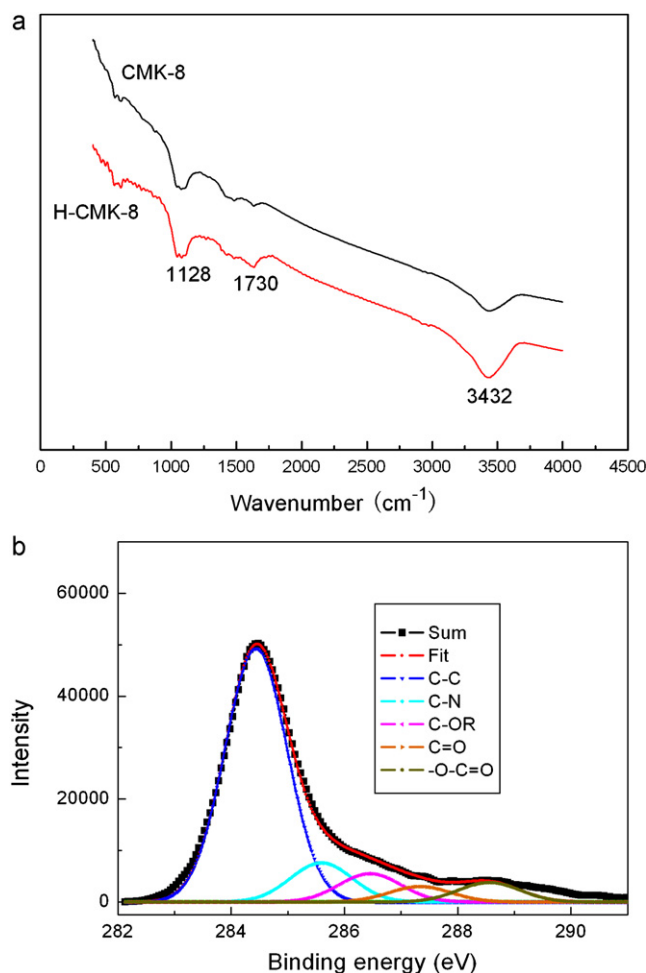

Fig. 3. (a) The FTIR spectra of the CMK-8 and the H-CMK-8 and (b) C$_{1s}$ XPS high-resolution spectra of H-CMK-8 carbon.
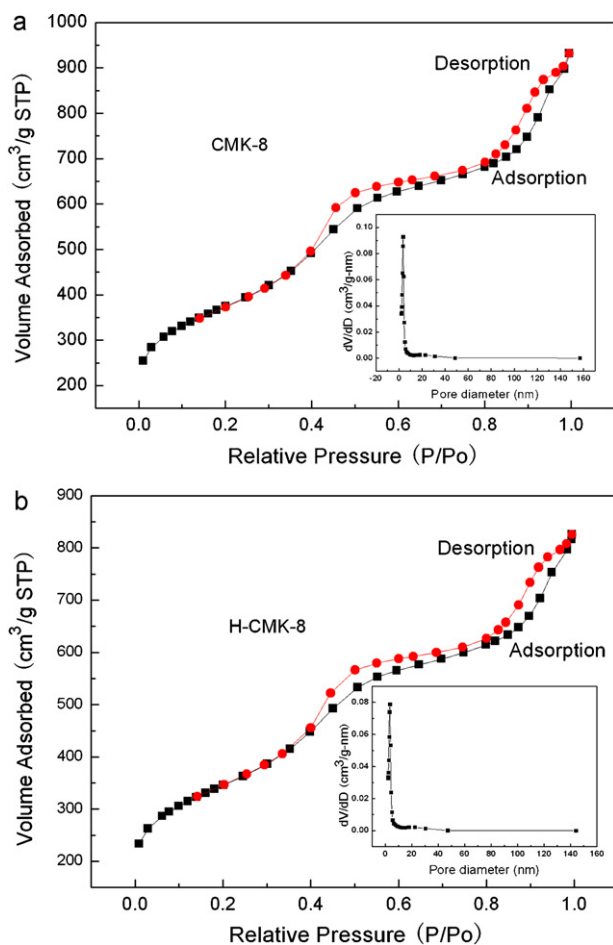
Fig. 4. N_2 adsorption–desorption isotherms of (a) the CMK-8 and (b) the H-CMK-8 carbons. The inset is the BJH pore-size distribution of the corresponding material.

Fig. 5. CV curves of (a) the CMK-8 and H-CMK-8 electrodes at sweep rate of $10\,mV\,s^{-1}$ and (b) the H-CMK-8 electrode at different sweep rates.

at around $3432\,cm^{-1}$ is observed in both the two samples, which is mainly caused by the O–H stretching vibration of the adsorbed water molecules. The broad band appeared at $1128\,cm^{-1}$ is caused by the stretching vibration of the C–O bonds. In addition, the C=O stretching vibrations related to carbonyl and/or carboxyl groups can be found around $1730\,cm^{-1}$ [31]. The spectrum of the H-CMK-8 is similar to that of the CMK-8 except for stronger intensity of the peak at $1730\,cm^{-1}$ for the H-CMK-8, indicating more oxygen-containing functional groups existing on the channel surface of the H-CMK-8.

From XPS test, it is confirmed that O (13.8 at.%) and N (0.97 at.%) were introduced during acid oxidation, and oxygen-containing C groups (including C–OR, C=O and –O–C=O) were formed meantime. The chemical nature of these functional groups was determined by deconvolution of the C_{1s} peak. As shown in Fig. 3b, the best fitting is invariably obtained with Gaussian lines. Deconvolution of C_{1s} spectrum gives five peaks representing carbon atoms bonded to carbon, nitrogen and oxygen atoms. These five peaks are related to C–C bond (284.4 eV), C–N bond (285.6 eV), C–OR (286.4 eV), C=O (287.3 eV) and –O–C=O (288.6 eV), respectively. The C–N, C–O, C=O and –O–C=O fractions are as high as 10.8 at.%, 7.79 at.%, 4.26 at.% and 5.5 at.% in H-CMK-8, respectively, indicating a significant amount of N- and O-containing groups. Actually, these nitrogen- and oxygen-containing functional groups, such as C–N group and pyrone-like functionalities (part of C=O and C–O) in the surfaces of nano-channels of the H-CMK-8 carbon can make effects on the electrochemical capacitive behaviors [32,33].
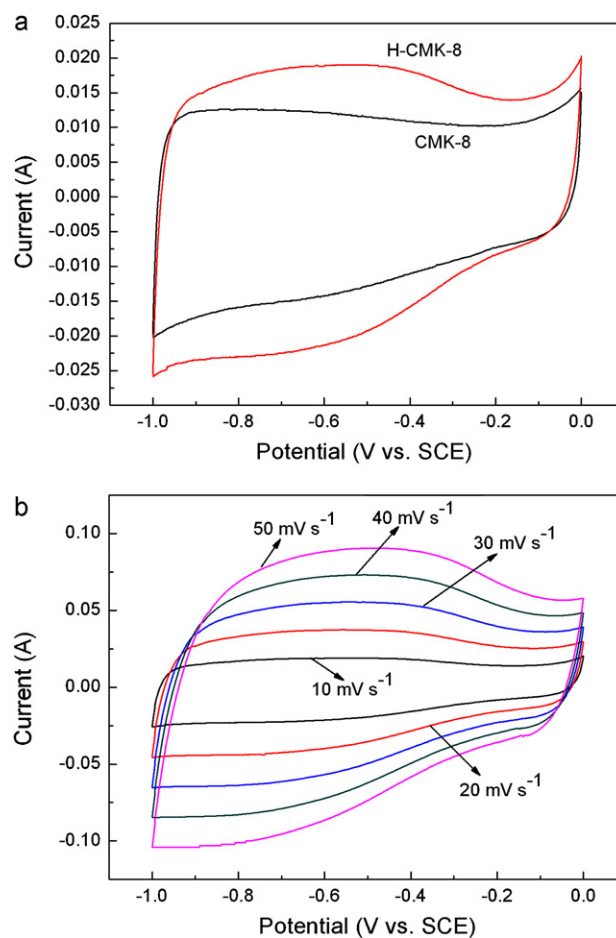
The specific surface area and pore-size distribution analyses of the CMK-8 and H-CMK-8 samples were conducted using N_2 adsorption and desorption experiments. Fig. 4a and b shows the N_2 adsorption–desorption isotherms of the CMK-8 and the H-CMK-8, respectively. The corresponding BJH pore-size distributions curve is shown in the insets. As seen from Fig. 4, the nitrogen sorption isotherms for the two samples are of type IV, although the hysteresis loops are of mixed types. The two samples both show high specific surface area, pore volume and narrow mesopore-size distribution. In detail, the BET surface area of the CMK-8 is $1321\,m^2\,g^{-1}$, the mesopore volume is $1.38\,cm^3\,g^{-1}$, and the average pore diameter is 4.78 nm. The BET surface area of the H-CMK-8 is $1217\,m^2\,g^{-1}$, the mesopore volume is $1.18\,cm^3\,g^{-1}$, and the pore diameter is 4.65 nm. It is obvious that the acid treatment leaded to the slight decrease in the specific surface area, pore volume and average pore size.

3.2. Electrochemical test

CV and chronopotentiometry measurements were employed to evaluate the electrochemical properties and to calculate the specific capacitances of as-prepared CMK-8 and H-CMK-8 electrodes. Fig. 5a shows the CV curves of the CMK-8 and the H-CMK-8 electrodes at the scan rate of $10\,mV\,s^{-1}$ between -1.0 and $0\,V$ (vs. SCE) in 2 M KOH aqueous electrolyte. It can be seen that the CV curve of the CMK-8 electrode shows a typical rectangular shape, no obvious Faradaic current is observed in the voltammogram [34]. Nevertheless, the CV curve of the H-CMK-8 electrode deviated from idealized double-layer behaviors with a pair of broad,
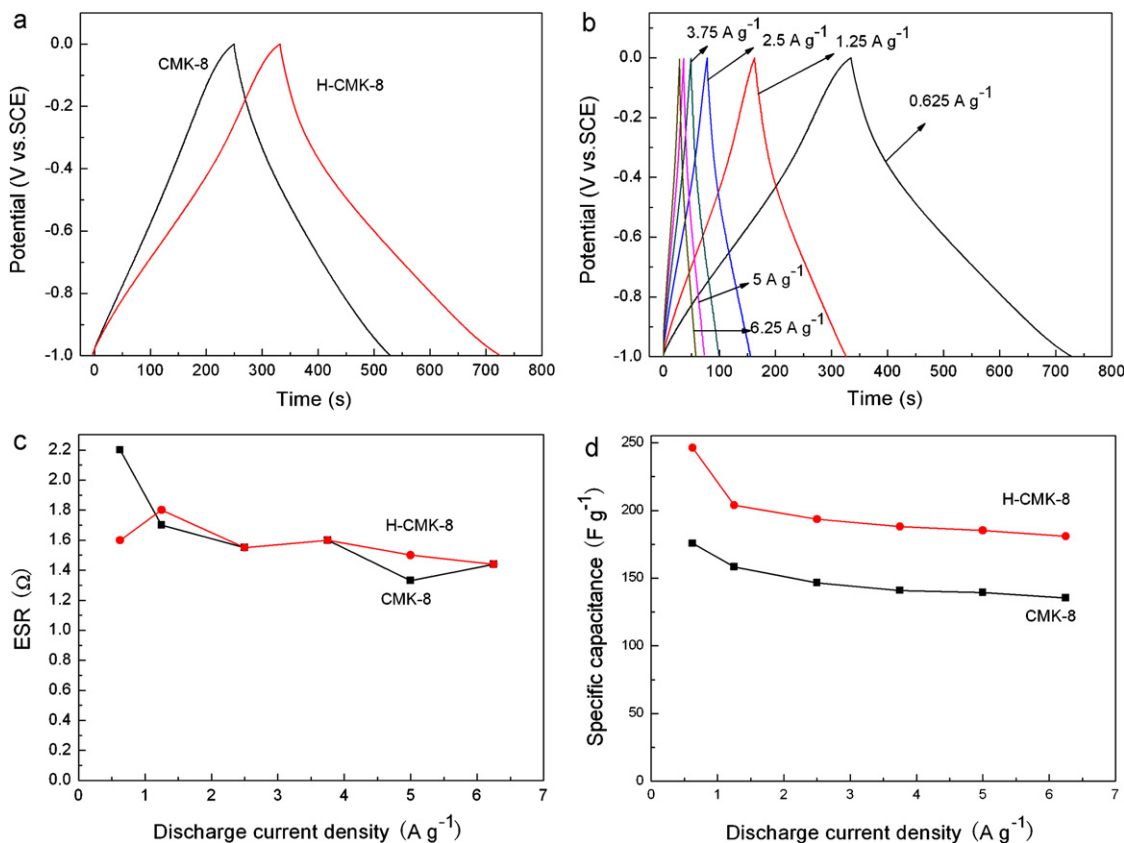
Fig. 6. (a) The charge–discharge curves of (a) the CMK-8 and H-CMK-8 electrodes at a current density of $0.625\,A\,g^{-1}$ and (b) H-CMK-8 electrode at different current densities; (c) the ESR as a function of discharging current density; (d) the specific capacitance of the CMK-8 and H-CMK-8 electrodes as a function of discharging current density.

superimposed and reversible faradaic surface redox reactions, behaving as pseudocapacitance. It was attributed to redox reactions of the N and O (pyrone-like) functionalities on the surface of the H-CMK-8 [32,33]. Moreover, it is clear that the H-CMK-8 electrode exhibits a larger CV area than that of the CMK-8 electrode, indicating a higher specific capacitance compared with the untreated CMK-8. It mainly because that the pseudo-capacitance obtained from the oxygenated groups improved the electrochemical properties of the CMK-8 carbon [35]. The specific capacitance value for the CMK-8 and H-CMK-8 electrodes which obtained from the CV curves in Fig. 5a according to formula (1) were 152 ($1.52\,A\,g^{-1}$) and 239 F g^{-1} ($2.4\,A\,g^{-1}$), respectively. Fig. 5b shows the CV curves of the H-CMK-8 electrode at different scan rates. No obvious distortion in the CV curves to be observed as the sweep rate increased, suggesting a highly reversible system in the KOH electrolyte within the potential range employed. However, with the increase of the sweep rate, the H-CMK-8 electrode has a small delay for the current to reach a horizontal value near the reversal of the potential sweep, reflecting a more significant ohmic resistance in pores.

Fig. 6a shows the charge/discharge curves of the CMK-8 and H-CMK-8 electrodes within a potential window of -1.0 to $0\,V$ at a current density of $0.625\,A\,g^{-1}$. Fig. 6b shows the charge–discharge curves of the H-CMK-8 electrode at different current densities. It is clear seen that the shape of the charge–discharge curves of the CMK-8 and H-CMK-8 electrode are closely linear and show a typical triangle symmetrical distribution, indicating a good double layer capacitive property. The electric efficiency is almost near 100% for the two carbon electrodes, indicating a high charge/discharge propagation, low resisitivity, and good reversible process. The voltage drop (IR) is associated with the equivalent series resistance (ESR) of the supercapacitor cell (IR $= I \times$ ESR). The ESR is the sum of internal resistance, including the electronic resistance

of electrode, the diffusing resistance of ions in the nanopores of electrode materials, and the interfacial resistance between the electrode and the current collector [36]. As shown in Fig. 6c, the CMK-8 and H-CMK-8 electrode both show very low ESR at different current densities. The specific capacitance values for the CMK-8 and H-CMK-8 electrodes which obtained from the charge/discharge curves in Fig. 6a according to formula (2) were 176 ($0.625\,A\,g^{-1}$) and 246 F g^{-1} ($0.625\,A\,g^{-1}$), respectively. These results suggested that the supercapacitor performance of the CMK-8 can be substantially improved by acid treatment. Although no obvious psedo-capacitance characteristic was observed in the charge/discharge curves of the H-CMK-8 electrode, we believe that the acid treatment of carbon surface yielded surface oxygen groups, which conduct complex faradic reactions and thus enhance the pseudocapacitance.

To further understand the high rate capability of the CMK-8 and H-CMK-8 electrodes, the charge/discharge measurements were recorded at different current densities. Fig. 6d reveals that the values of the specific capacitance for the CMK-8 and H-CMK-8 electrodes are strongly dependent on the current density. In detail, the specific capacitance slightly decreases with the increase of the current density. Up to a relatively large current density of $6.25\,A\,g^{-1}$, nearly 77 and 74% of the initial value is remained for the CMK-8 and the H-CMK-8, respectively. Although the capacitance retention of H-CMK-8 is slightly smaller than that of the CMK-8, the specifica capacitance of the H-CMK-8 at $6.25\,A\,g^{-1}$ is 181 F g^{-1}, which is still much higher than that of CMK-8 (135 F g^{-1}) at the same current density. It indicates that the high rate capability of the CMK-8 can be preserved after surface acid treatment. The result also shows that the the CMK-8 and H-CMK-8 electrodes allow rapid ion diffusion and exhibit good electrochemical utilization. Here, the unique 3D mesoporous network can facilitate ion transport throughout
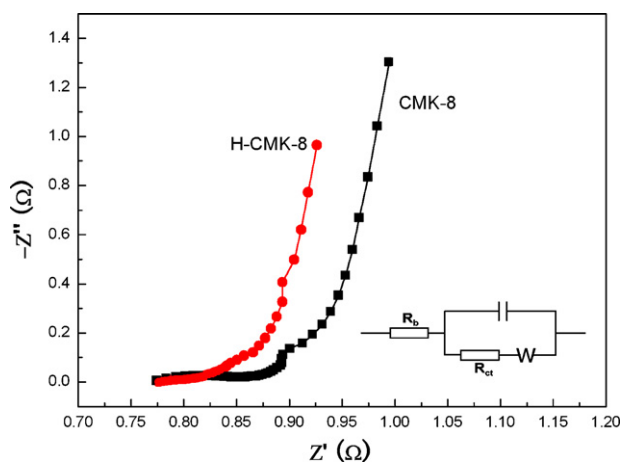
Fig. 7. Complex-plane impedance plots of the CMK-8 and H-CMK-8 electrodes. The inset is the equivalent circuit.

Fig. 8. Cycle life of the CMK-8 and H-CMK-8 electrodes at the current densities of $1.25\,A\,g^{-1}$.

the pore channels without pore blockage, which makes the surface of CMK-8 carbon favorable for charging the electric double-layer.

As a powerful technique for the investigation of the capacitive behavior of the supercapacitor cells, EIS was used to check the ability of 3D cubic mesoporous carbon to store electrical energy in our case. The complex plane plots of the AC impedance spectra for the CMK-8 and the H-CMK-8 were shown in Fig. 7. It is seen that the plots both exhibit two distinct traits: a semicircle in the high frequency range and a sloped line in the low frequency range. Moreover, a distinct knee in the frequency is observed in each curve. From the point intersecting with the real axis in the range of high frequency, the internal resistance (which is equal to R_b) of the electrode material includes the total resistances of the ionic resistance of the electrolyte, the intrinsic resistance of active materials, and the contact resistance at the active material/current collector interface. The semicircle in the high-frequency range associates with the surface properties of the porous electrode, which corresponds to the faradic charge transfer resistance (R_{ct}). At the lower frequencies, a straight sloping line represents the diffusive resistance (warburg impendence) of the electrolyte in electrode pores and the proton diffusion in host material. It should be mentioned that the two carbon electrodes have the same small R_b. Nevertheless, there is still obvious difference existing between the two spectra. The semicircle of the H-CMK-8 is smaller than that of the CMK-8, indicating the lower impedance on electrode/electrolyte interface. Moreover, two spectra both show a Warburg angle higher than 45°, indicating the suitability of the cubic mesoporous carbon as the electrode materials for supercapacitors [37,38].

The cycle life of the CMK-8 and H-CMK-8 electrodes was monitored by a chronopotentiometry measurement at $1.25\,A\,g^{-1}$ in 2 M KOH electrolyte. As shown in Fig. 8, at the initial stage, the specific capacitance of the CMK-8 and H-CMK-8 electrodes both decrease gradually with the increase of the cycle number. After the beginning 200 cycling, for the CMK-8 electrode, the value of the specific capacitance is $150\,F\,g^{-1}$ which is 85% of the initial value; and for the H-CMK-8 electrode, the value of the specific capacitance is $199\,F\,g^{-1}$ which is 81% of the initial value. After that, the specific capacitance for the CMK-8 is almost no decay up to 2000 cycles, and for the H-CMK-8, the specific capacitance only shows 6% decay. This demonstrates that, within the voltage window −1.0–0 V, the repeating charge–discharge behavior did not seem to induce the significant structural change for the CMK-8 and H-CMK-8 electrodes. The long-term stability implies that the CMK-8, the H-CMK-8 especially, is an excellent electrode material for supercapacitors.
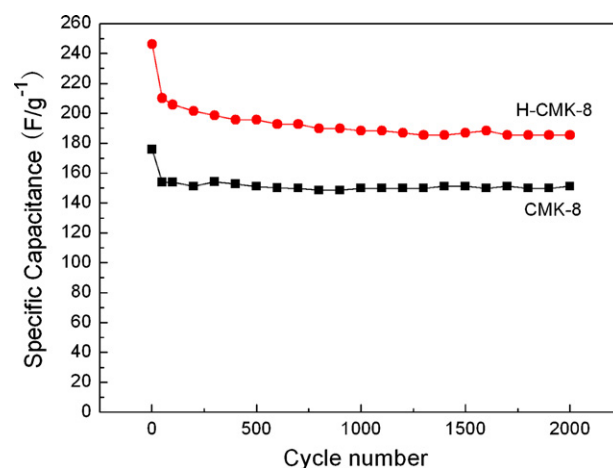
4. Conclusions

In summary, the ordered cubic mesoporous CMK-8 was synthesized using KIT-6 as hard template and its surface chemical modification was employed by nitric acid treatment. The CMK-8 and H-CMK-8 electrodes both possess good supercapacitive properties due to the interconnected 3D mesoporous network, which can facilitate ion diffusion throughout the pore channels without pore blockage. The supercapacitor performance of the CMK-8 can be substantially improved by acid treatment and the H-CMK-8 electrode shows the largest specific capacitance of $246\,F\,g^{-1}$ at $0.625\,A\,g^{-1}$. Also, two electrodes exhibit good cycling stability and lifetime as well. These encouraging results illustrate the exciting potential for high performance supercapacitors based on such ordered 3D mesoporous carbon materials.

Acknowledgement

References

[1] M. Winter, R.J. Brodd, Chem. Rev. 104 (2004) 4245–4269.
[2] S.L. Xiong, C.Z. Yuan, X.G. Zhang, B.J. Xi, Y.T. Qian, Chem. Eur. J. 15 (2009) 5320–5326.
[3] B.E. Conway, Electrochemical Supercapacitors Scientific Fundamentals and Technological Applications, Kluwer Academic/Plenum Publishers, New York, 1999.
[4] Z.S. Wu, D.W. Wang, W.C. Ren, J.P. Zhao, G.M. Zhou, F. Li, H.M. Cheng, Adv. Funct. Mater. 20 (2010) 3595–3602.
[5] J.W. Lang, L.B. Kong, W.J. Wu, Y.C. Luo, L. Kang, Chem. Commun. 35 (2008) 4213–4215.
[6] C.G. Liu, Z.N. Yu, D. Neff, A. Zhamu, B.Z. Jang, Nano Lett. 10 (2010) 4863–4868.
[7] H.L. Wang, H.S. Casalongue, Y.Y. Liang, H.J. Dai, J. Am. Chem. Soc. 21 (2010) 7472–7477.
[8] J.W. Lang, L.B. Kong, M. Liu, Y.C. Luo, L. Kang, J. Electrochem. Soc. 157 (2010) A1341–A1346.
[9] F.H. Li, J.F. Song, H.F. Yang, S.Y. Gan, Q.X. Zhang, D.X. Han, A. Ivaska, L. Niu, Nanotechnology 20 (2009) 455602 (6 pp).
[10] H. Zhang, G.P. Cao, Z.Y. Wang, Y.S. Yang, Z.J. Shi, Z.N. Gu, Electrochem. Commun. 10 (2008) 1056–1059.
[11] X.B. Yan, J.T. Chen, J. Yang, Q.J. Xue, P. Miele, ACS Appl. Mater. Interface 2 (2010) 2521–2529.
[12] M.D. Stoller, S. Park, Y.W. Zhu, J.H. An, R.S. Ruoff, Nano Lett. 8 (2008) 3498–3502.
[13] C.T. Hsieh, Y.T. Lin, Micropor. Mesopor. Mater. 93 (2006) 232–239.
[14] W. Lu, L.T. Qu, K. Henry, L.M. Dai, J. Power Sources 189 (2009) 1270–1277.
[15] V.V. Panic, R.M. Stevanovic, V.M. Jovanovic, A.B. Dekanski, J. Power Sources 181 (2008) 186–192.
[16] Y. Chen, X. Zhang, D.C. Zhang, P. Yu, Y.W. Ma, Carbon 49 (2011) 573–580.

[17] L. Yu, C.X. Zhao, X. Long, W. Chen, Micropor. Mesopor. Mater. 126 (2009) 58–64.
[18] H.J. Liu, X.M. Wang, W.J. Cui, Y.Q. Dou, D.Y. Zhao, Y.Y. Xia, J. Mater. Chem. 20 (2010) 4223–4230.
[19] Q.H. Guo, X.P. Zhou, X.Y. Li, S.L. Chen, A. Seema, A. Greiner, J. Mater. Chem. 19 (2009) 2810–2816.
[20] L.X. Li, H.H. Song, X.H. Chen, Electrochim. Acta 51 (2006) 5715–5720.
[21] X.C. Zhao, A.Q. Wang, J.W. Yan, G.Q. Sun, L.X. Sun, T. Zhang, Chem. Mater. 22 (2010) 5463–5473.
[22] H.F. Li, R.D. Wang, R. Cao, Micropor. Mesopor. Mater. 111 (2008) 32–38.
[23] D.C. Wu, X. Chen, S.H. Lu, Y.R. Liang, F. Xu, R.W. Fu, Micropor. Mesopor. Mater. 131 (2010) 261–264.
[24] H.F. Li, S.M. Zhu, H.A. Xi, R.D. Wang, Micropor. Mesopor. Mater. 89 (2006) 196–203.
[25] J. Zhang, L.B. Kong, J.J. Cai, H. Li, Y.C. Luo, L. Kang, Micropor. Mesopor. Mater. 132 (2010) 154–162.
[26] J.C. Wang, X.F. Yu, Y.X. Li, Q. Liu, J. Phys. Chem. C 111 (2007) 18073–18077.
[27] M. Lezanska, J. Wloch, G. Szymanski, I. Szpakowska, J. Kornatowski, Catal. Today 150 (2010) 77–83.
[28] K.P. Gierszal, M. Jaroniec, T.W. Kim, J. Kim, R. Ryoo, New J. Chem. 32 (2008) 981–993.
[29] M. Oschatz, E. Kockrick, M. Rose, L. Borchardt, N. Klein, I. Senkovska, T. Freudenberg, Y. Korenblit, G. Yushin, S. Kaskel, Carbon 48 (2010) 3987–3992.
[30] L.B. Kong, J.W. Lang, M. Liu, Y.C. Luo, L. Kang, J. Power Sources 194 (2009) 1194–1201.
[31] J. Zhang, L.B. Kong, J.J. Cai, Y.C. Luo, L. Kang, Electrochim. Acta 55 (2010) 8067–8073.
[32] M.P. Bichat, E. Raymundo-Piñero, F. Béguin, Carbon 48 (2010) 4351–4361.
[33] V. Khomenko, E. Raymundo-Piñero, F. Béguin, J. Power Sources 195 (2010) 4234–4241.
[34] Q.L. Du, M.B. Zheng, L.F. Zhang, Y.W. Wang, J.H. Chen, L.P. Xue, W.J. Dai, G.B. Ji, J.M. Cao, Electrochim. Acta 55 (2010) 3897–3903.
[35] F. Lufrano, P. Staiti, Energy Fuels 24 (2010) 3313–3320.
[36] Z.B. Lei, N. Christov, X.S. Zhao, Energy Environ. Sci. 4 (2011) 1866–1873.
[37] M.W. Xu, D.D. Zhao, S.J. Bao, H.L. Li, J. Solid State Electrochem. 11 (2007) 1101–1107.
[38] S.S. Zhang, K. Xu, T.R. Jow, Electrochim. Acta 49 (2004) 1057–1061.